Physics Letters A 381 (2017) 2214–2221

Contents lists available at ScienceDirect

Physics Letters A

www.elsevier.com/locate/pla

Dynamics and scaling properties for a one-dimensional impact system with two periodically vibrating walls

André L.P. Livorati [a,b,*]

[a] Departamento de Física, UNESP – Univ Estadual Paulista, Av. 24A, 1515 – Bela Vista, 13506-900, Rio Claro, SP, Brazil
[b] School of Mathematics, University of Bristol, Bristol, BS8 1TW, United Kingdom

ARTICLE INFO

Article history:
Received 8 November 2016
Received in revised form 16 March 2017
Accepted 22 April 2017
Available online 9 May 2017
Communicated by F. Porcelli

Keywords:
Scaling
Diffusion
Nonlinear mapping
Impact system

ABSTRACT

We investigate the dynamics of a system composed of a particle suffering impacts between two heavy periodically vibrating walls. An original, nonlinear area preserving mapping is obtained. The control parameters of amplitude of perturbation and frequency of oscillation play an important role in the phase space, shaping the portion of chaotic seas, position of invariant curves and the amount of KAM islands. The study of the behavior of the root mean square velocity was made via analytical description and numerical simulations. We proposed scaling arguments to describe its dynamics and our results show remarkably good agreement between the theory and the simulations concerning a scaling invariance with respect to the control parameters. Also, an analysis of the diffusion coefficient confirms the validity of the scaling invariance, giving robustness to our modeling.

1. Introduction

Hamiltonian dynamical systems with moving boundaries have been studied for a long time [1–3], where their dynamics are typically non-ergodic and non-integrable. These systems present mixed dynamics in the phase space, with KAM islands, invariant tori, spanning curves and chaotic seas, where the interface between them is very complex and not yet fully understood. Also, depending on both of the initial conditions as well as control parameters, such systems may present very rich and hence complex dynamics, therefore leading to a huge variety of nonlinear phenomena [4–6]. Considering their dynamics, in either dissipative or non-dissipative regimes [7–13], an analysis of scaling arguments and statistical properties yields new approaches, new formalisms, therefore moving forward the progress of the nonlinear science.

Our main goal in this paper is to introduce the dynamics of a system where a single particle (or an ensemble of non-interacting particles), suffers elastic impacts inside a closed domain bordered by two heavy periodically moving walls. The motivation for this model backs to Ulam [14] and Fermi [15], who developed a prototype model in order to explain the high energy of the cosmic rays, known as Fermi–Ulam model (FUM) [12], where an impact mechanism was setup, considering a particle suffering collision between two walls, where one is fixed and the other is periodically vibrating. Such a moving boundary system can be considered as billiard-like dynamical system [2,16,17]. Applications in different areas of research can be found such as: granular materials [18,19], microwaves [20], quantum dots [21,22], synchronization [23], mechanical vibrations [24,25], laser dynamics [26], chaos control [27,28], astrophysics [29], atom-optics [30,31], quantum effects [32,33], experimental devices [34,35], among many others.

This dynamical system that we aim to introduce in this paper differs from the original FUM [36–39]. Here, we are considering that the particle bounces between two heavy periodically vibrating walls, where each one of them has its own independent frequency of oscillation and amplitude of perturbation. Indeed, the kind of dynamics that we are proposing may be interpreted as a modeling for some known physical applications, such as ratchet-like dynamics [40–42], where the connection with our modeling comes from an interaction of the particle with two driven periodic oscillators, i.e., both vibrating walls. Another examples are: the photonic laser thruster, where a laser beam suffers successive reflections among moving mirrors [43–45], as well as classic and quantum δ-kicked rotators [46–50].

The dynamics of our proposed impact system is described by an original, nonlinear and area preserving mapping, which has four nonlinear terms and three control parameters and makes the mapping unique among similar impact dynamical systems present in the literature. The phase space presents mixed properties, with chaotic seas, invariant curves and KAM islands, where the ratio between frequencies of oscillation, influences the number of islands

* Correspondence to: Departamento de Física, UNESP – Univ Estadual Paulista, Av. 24A, 1515 – Bela Vista, 13506-900, Rio Claro, SP, Brazil.
E-mail address: livorati@usp.br.

http://dx.doi.org/10.1016/j.physleta.2017.04.042
0375-9601/

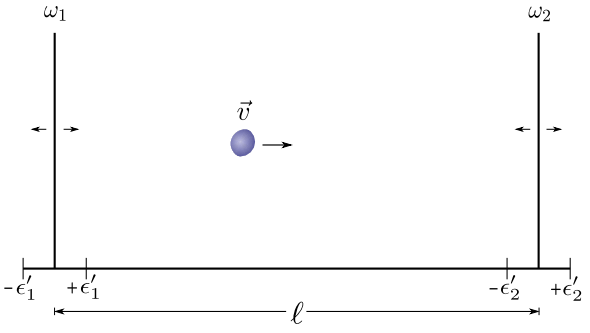

Fig. 1. Illustration of the dynamics of the impact system and its variables.

and the size of the chaotic sea. Because of this last property, the system denotes potential for further investigations concerning transport analysis, stickiness influence and anomalous diffusion [7,8,11,12]. Also, if one could introduce dissipation to the dynamics, we believe that crises between attractors [9] and self-similarity structures in the parameter space would be observed. So, in a primary study of our impact system, the behavior of the root mean square velocity was investigated, where an analytical description of its evolution was made. Our numerical simulations lead us to propose scaling arguments to describe the dynamics of the root mean square velocity. At the end, an universal collapse for these curves was obtained, which gives validity to our scaling hypothesis. Also, an analysis concerning the diffusion coefficient was made and shows a remarkable agreement with the analytical argument obtained by the investigation of the root mean square velocity as a function of the control parameters. Such agreement gives robustness to the modeling of our dynamical system.

The paper is organized as follows: in Sec. 2 we describe how the mapping was obtained and some dynamical and chaotic properties. Section 3 is devoted to discussing the behavior of the root mean square velocity via analytical investigation and numerical simulations. It also describes the scaling invariance of the root mean square velocity curves regarding the control parameters. Yet, an analysis of the diffusion coefficient also confirms the validity of the analytical investigations and of the scaling arguments. Finally in Sec. 4, we present our final remarks and conclusions.

2. The model and the mapping

The dynamical system under study in the paper basically consists of a particle of mass m moving in straight line trajectories, confined in a region of length ℓ, where in each boundary of this confined region, lies two heavy periodically moving walls. The velocity of the particle is said to be constant during the "flight time". It only changes, when the particle interacts with the moving walls. Fig. 1 displays a schematic illustration of the dynamical system and its variables.

In both heavy moving walls, the periodicity is given by a cosine function. Their equations of motion are $x_{w1} = \epsilon_1' \cos(\omega_1 t)$ for the left hand-side wall, said to be wall-1, and $x_{w2} = \epsilon_2' \cos(\omega_2 t)$ for the right hand side wall, said to be wall-2. Here, ϵ_1', ϵ_2', ω_1 and ω_2 are the respectively amplitudes of motion and frequencies of oscillation.

The collision scenario will be setup considering the static wall approximation (SWA) [36,37], where no transcendental equations must be solved to find the exact collision time. In this approximation both walls are said to be fixed (at rest), but the particle exchanges momentum and energy with the walls at each collision as if they were moving normally [51,52]. It had been shown before that in similar impact dynamical systems, the difference between the real dynamics and the SWA is nearly null, if one considers the whole accessible phase space [8,51].

The mapping dynamics will be described in the variables velocity v and time t. As an initial condition, we considered that the particle belongs to the wall-1, with an initial velocity v_0 with positive orientation and the initial time t_0. Once we decided to choose wall-1 as an initial condition (one could also start with wall-2, without any loss of generality), the mapping dynamics will be updated each time the particle collides again with wall-1.

Since we are considering static wall approximation, the time elapsed until the collision with the wall-2 can be set as $t_{1,2} = t_0 + \ell/v_0$. In the same manner, the return time will be $t_{2,1} = -\ell/v_1$, where now v_1 is the velocity of the particle after colliding with wall-2 and it has negative orientation. So the total time for the particle to leave wall-1, collide with wall-2, and come back to collide with wall-1 again is $t_t = t_{1,2} + t_{2,1}$, which gives us

$$t_t = t_0 + \ell \left[\frac{v_1 - v_0}{v_0 v_1} \right] . \tag{1}$$

Let us now obtain the expression for v_1. To evaluate the exchange of momentum and energy at each collision, we must consider a change in the reference frame, from inertial to non-inertial. So, one may consider $\vec{X}(t_0) = \vec{x_p}'(t_0) + \vec{x_{w2}}(t_{1,2})$, where $\vec{x_p}'$ is the position of the particle in the non-inertial reference frame, $\vec{x_{w2}}$ and $\vec{X}$ are respectively the equation of the wall-2 and the particle position in the inertial reference frame. After a time derivative we found $\vec{V}(t_0) = \vec{v_p}'(t_0) + \vec{v_{w2}}(t_{1,2})$. The term $\vec{v_p}'(t_0)$, is setup before the collision with wall-2 happens.

After the collision, and considering the conservation of momentum, one obtain $\vec{v_p}'(t_{1,2}) = -\vec{v_p}'(t_0)$. Coming back to the inertial reference frame, one may find $\vec{V}(t_{1,2}) = \vec{v_p}'(t_{1,2}) + \vec{v_{w2}}(t_{1,2})$. Rearranging properly the terms and setting $\vec{V}(t_{1,2}) = v_1$, $\vec{V}(t_0) = v_0$ and $\vec{x_{w2}}(t_{1,2}) = -\epsilon_2' \omega_2 \sin(\omega_2 t_{1,2})$, one can finally obtain

$$v_1 = -v_0 - 2\epsilon_2' \omega_2 \sin(\omega_2 t_{1,2}) . \tag{2}$$

Coming back to the total flight time expression set in Eq. (1), and replacing the expression for v_1 obtained in Eq. (2), one may find

$$t_t = t_0 + \ell \left[\frac{-v_0 - 2\epsilon_2' \omega_2 \sin(\omega_2 t_{1,2}) - v_0}{v_0(-v_0 - 2\epsilon_2' \omega_2 \sin(\omega_2 t_{1,2}))} \right] .$$

Rearranging the terms from the above expression, one may obtain

$$t_t = t_0 + 2\ell \left[\frac{1 + \frac{\epsilon_2' \omega_2}{v_0} \sin(\omega_2 t_{1,2})}{v_0 + 2\epsilon_2' \omega_2 \sin(\omega_2 t_{1,2})} \right] . \tag{3}$$

Since we are evaluating the dynamics considering a total flight time from wall-1, until the particle collides again with it, we should set the velocity v_2 when the particle returns to the wall-1. So, applying the same procedure as done for v_1 one may obtain

$$v_2 = -v_1 - 2\epsilon_1' \omega_1 \sin(\omega_1 t_t) . \tag{4}$$

Replacing Eq. (2) into Eq. (4) and properly naming the terms: $v_0 = v_n$, $v_2 = v_{n+1}$, $t_t = t_{n+1}$ and $t_0 = t_n$, one may find

$$T : \begin{cases} v_{n+1} = v_n + 2\epsilon_2' \omega_2 \sin(\omega_2 t_{1,2}) - 2\epsilon_1' \omega_1 \sin(\omega_1 t_t) \\ t_{n+1} = t_n + 2\ell \left[\frac{1 + \frac{\epsilon_2' \omega_2}{v_n} \sin(\omega_2 t_{1,2})}{v_n + 2\epsilon_2' \omega_2 \sin(\omega_2 t_{1,2})} \right] \end{cases} . \tag{5}$$

One can realize that in Eq. (5) there are too many control parameters in the mapping, ϵ_1', ϵ_2', ω_1, ω_2 and ℓ. In order to reduce these control parameters, let us set some dimensionless parameters as $\epsilon_1 = \epsilon_1'/\ell$, $\epsilon_2 = \epsilon_2'/\ell$, and $\tilde{\omega} = \omega_2/\omega_1$. Also, since we are considering the mapping update when the particle reaches wall-1, let us set a dimensionless velocity as $V_n = v_n/\omega_1 \ell$ and measure

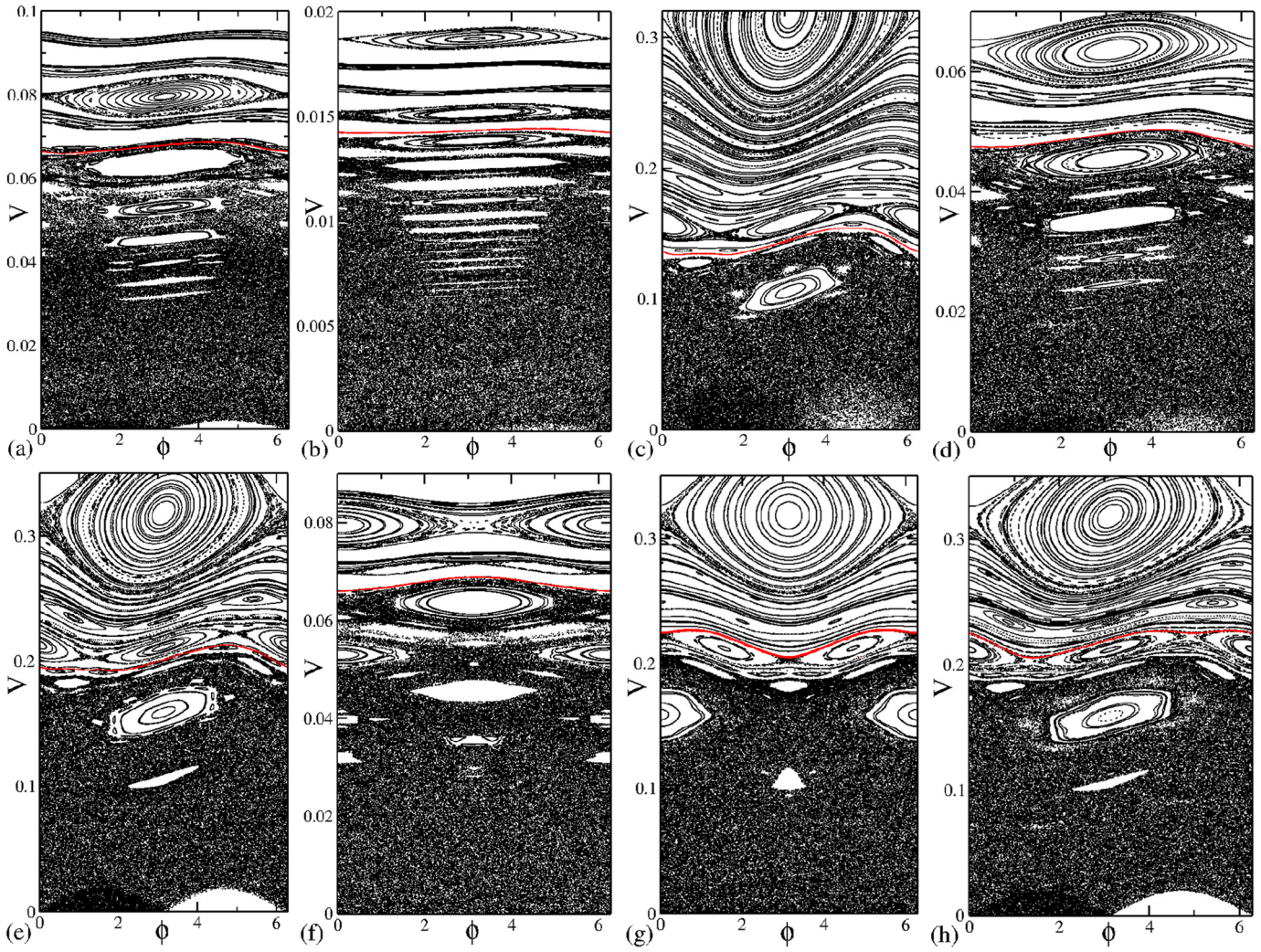

Fig. 2. Snapshots of the phase space (ϕ, V) for the impact system. The control parameters used were: (a) $\epsilon_1 = 0.001$ and $\epsilon_2 = 0$; (b) $\epsilon_1 = \epsilon_2 = 0.0001$; (c) $\epsilon_1 = \epsilon_2 = 0.01$; (d) $\epsilon_1 = \epsilon_2 = 0.001$; (e) $\epsilon_1 = 0.01$ and $\epsilon_2 = 0.001$; (f) $\epsilon_1 = 0.0001$ and $\epsilon_2 = 0.001$; (g) $\epsilon_1 = 0.0001$ and $\epsilon_2 = 0.01$; and finally (h) $\epsilon_1 = 0.01$ and $\epsilon_2 = 0.0001$. Also, in all items of the figure we set $\tilde{\omega} = 1$, and positions of the first invariant spanning curve is displayed in red in all items.

the time according $\phi_n = \omega_1 t_n$. After rearranging the terms properly, one may obtain a dimensionless mapping with three control parameters as

$$T : \begin{cases} V_{n+1} = |V_n + 2\epsilon_2 \tilde{\omega} \sin(\tilde{\omega}\tilde{\Phi}) - 2\epsilon_1 \sin(\phi_{n+1})| \\ \phi_{n+1} = \phi_n + 2\left[\frac{1+\frac{\epsilon_2 \tilde{\omega}}{V_n} \sin(\tilde{\omega}\tilde{\Phi})}{V_n + 2\epsilon_2 \tilde{\omega} \sin(\tilde{\omega}\tilde{\Phi})}\right] \bmod (2\pi) \end{cases}, \tag{6}$$

where the term $\tilde{\Phi} = \phi_n + (1/V_n)$ represents the dimensionless time $t_{1,2}$, and $\tilde{\omega}$ sets a ratio between the frequencies of oscillation of both walls as $\tilde{\omega} = \omega_2/\omega_1$. Also, the absolute value for V_{n+1} comes from the static wall approximation and prevents the particle going beyond wall-1, since a negative velocity would necessarily produce a non-physical situation.

Fig. 2 shows the phase space for different combinations of control parameters where we evaluated 225 different initial conditions evolved up to 10^3 iterations of Eq. (6). Since we have three control parameters, let us in principle range ϵ_2 and ϵ_1, and set $\tilde{\omega} = 1$ fixed. One can check that if we set $\epsilon_2 = 0$, the mapping recovers the simplified Fermi–Ulam model [52,53] displayed in Fig. 2(a), which guarantees the validity of Eq. (6). Continuing to range ϵ_1 and ϵ_2, one can realize that the phase space has basically the same structure. It presents mixed properties with a chaotic sea for lower velocities and invariant curves and local chaotic seas for higher velocities.

The range of both ϵ_1 and ϵ_2 defines the size of the finite portion of the lower chaotic sea. For Figs. 2(b,c,d), where we range $\epsilon_2 = \epsilon_1$ by two orders of magnitude, the phase space is similar to the regular FUM [12] when we consider the same value for the respective control parameter. Also, the position of first invariant spanning curve is displayed in red for all items of Fig. 2, and it plays the role of a limiting structure for the lower portion of the chaotic sea.

In Figs. 2(e,g), where $\epsilon_2 > \epsilon_1$, and in Figs. 2(f,h), where $\epsilon_1 > \epsilon_2$ the display of the stability islands changes, and the size of the lower portion of the chaotic sea obeys the bigger value among ϵ_1 and ϵ_2. As one can see, in Figs. 2(g,h) the position of the first invariant spanning curve, is the same for both phase spaces, considering a difference of two orders of magnitude between ϵ_1 and ϵ_2. The only notorious difference is a shift in the ϕ range and the appearance of different chains of islands.

Ranging the value of $\tilde{\omega}$, one can realize that there is a significant change in the phase space configuration, as shown in Fig. 3. The number of stability islands obeys in a linear way the range of $\tilde{\omega}$. For instance, in Fig. 3(a), we have $\epsilon_2 = \epsilon_1 = 0.01$ and $\tilde{\omega} = 3$. If one compares it with Fig. 2(c) which below has the same values of ϵ_1 and ϵ_2, the major island in the chaotic sea has now become three islands. The same occurs for different regular structures in the chaotic sea, (b) and above the first invariant spanning curve.

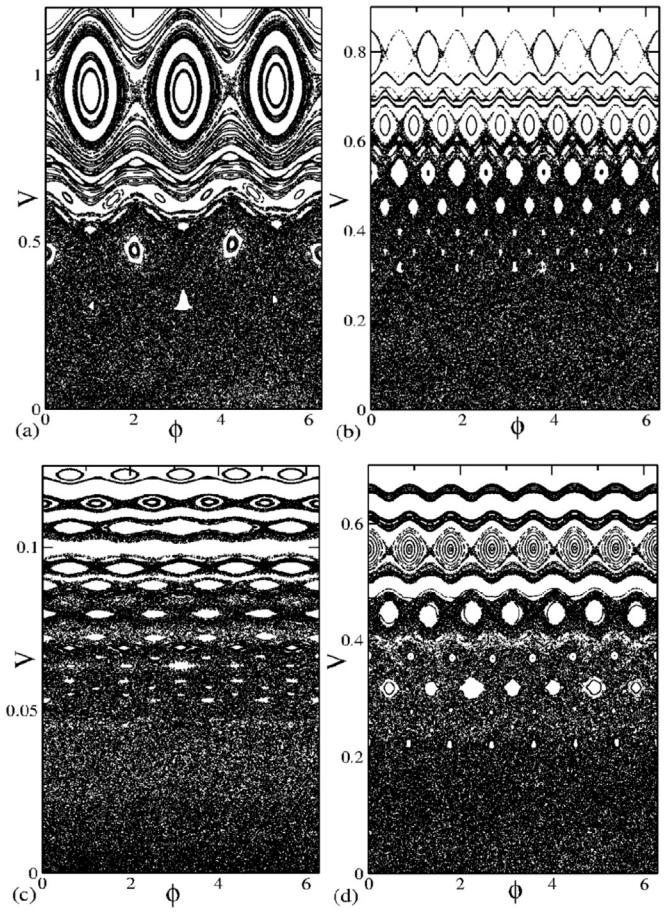

Fig. 3. Phase space considering a range of $\tilde{\omega}$. In (a) we have $\epsilon_1 = \epsilon_2 = 0.01$ and $\tilde{\omega} = 3$, in (b) $\epsilon_1 = \epsilon_2 = 0.001$ and $\tilde{\omega} = 10$, $\epsilon_1 = \epsilon_2 = 0.0001$ and $\tilde{\omega} = 5$, and finally in (d) $\epsilon_1 = \epsilon_2 = 0.001$ and $\tilde{\omega} = 7$. As one can see, the periodicity of the regular regions obeys the value of $\tilde{\omega}$ in a linear way.

Also, the portion of the chaotic sea which the particle is allowed to visit also increases with the increment of $\tilde{\omega}$.

Increasing the value of $\tilde{\omega}$, and also ranging the values of ϵ_1 and ϵ_2, one can realize from Figs. 3(b,c,d) a huge number of islands in the phase space. Comparing Fig. 2(d) with Figs. 3(b,d), which has the same values for ϵ_1 and ϵ_2, but with respectively $\tilde{\omega} = 1$, $\tilde{\omega} = 10$ and $\tilde{\omega} = 7$, one can see that the islands were substantially increased, where period-1 islands in Fig. 2(d), become period-10 and period-7 respectively in Figs. 3(b,d). Also, the same applies for multiple island regions, their respective cantori and satellite islands. This is clear evidence that the periodicity of stable orbits depends explicitly on $\tilde{\omega}$.

The phase space volume element transforms according to the determinant of the Jacobian matrix, whose elements are given by the partial derivatives of the mapping coordinates, as the following

$$J = \begin{pmatrix} \frac{\partial V_{n+1}}{\partial V_n} & \frac{\partial V_{n+1}}{\partial \phi_n} \\ \frac{\partial \phi_{n+1}}{\partial V_n} & \frac{\partial \phi_{n+1}}{\partial \phi_n} \end{pmatrix} , \tag{7}$$

where each element is given by

$$\frac{\partial V_{n+1}}{\partial V_n} = 1 + 2\tilde{\omega}^2\epsilon_2 \cos(\tilde{\omega}\tilde{\Phi})\frac{\partial \tilde{\Phi}}{\partial V_n} - 2\epsilon_1 \cos(\phi_{n+1})\frac{\partial \phi_{n+1}}{\partial V_n} ,$$

$$\frac{\partial V_{n+1}}{\partial \phi_n} = 2\tilde{\omega}^2\epsilon_2 \cos(\tilde{\omega}\tilde{\Phi})\frac{\partial \tilde{\Phi}}{\partial \phi_n} - 2\epsilon_1 \cos(\phi_{n+1})\frac{\partial \phi_{n+1}}{\partial \phi_n},$$

$$\frac{\partial \phi_{n+1}}{\partial V_n} = \left[\frac{A\frac{\partial \tilde{\Phi}}{\partial V_n} - B}{V_n C}\right] - 2\left[(1+B)\left(1 + A\frac{\partial \tilde{\Phi}}{\partial V_n}\right)\right]/C^2,$$

$$\frac{\partial \phi_{n+1}}{\partial \phi_n} = 1 + \left[\frac{A\frac{\partial \tilde{\Phi}}{\partial \phi_n}}{V_n C}\right] - 2\left[(1+B)\left(A\frac{\partial \tilde{\Phi}}{\partial \phi_n}\right)\right]/C^2 ,$$

with the auxiliary variables and derivatives as

$$\frac{\partial \tilde{\Phi}}{\partial V_n} = -\frac{1}{{V_n}^2} ,$$

$$\frac{\partial \tilde{\Phi}}{\partial \phi_n} = 1 ,$$

$$A = 2\tilde{\omega}^2\epsilon_2 \cos(\tilde{\omega}\tilde{\Phi}) ,$$

$$B = \frac{\tilde{\omega}\epsilon_2}{V_n}\sin(\tilde{\omega}\tilde{\Phi}) ,$$

$$C = V_n + 2\epsilon_2\tilde{\omega}\sin(\tilde{\omega}\tilde{\Phi}) .$$

One can check, after some straightforward algebra, that the determinant of the Jacobian matrix is equal to the unity, which includes our dynamical system in the class of the area preserving mappings [1,2].

3. Results ans discussion

In this section we will focus on and discuss some statistical and numerical results for the velocity of the particle, where scaling arguments were used to describe the dynamical scenario. Also, an analysis concerning the diffusion along the dynamical evolution is evaluated.

3.1. Root mean square velocity (V_{RMS}) and scaling analysis

Let us start evaluating the dynamics considering the velocity of the particle and its dynamical evolution as the number of collisions evolve. Since the sine function is present in the mapping (6), a direct average over an ensemble of the phase $\phi \in [0, 2\pi]$ is not convenient. Instead, we look at the squared velocity, hence allowing us to estimate the behavior of average squared velocity as a function of n. From the velocity equation of mapping in Eq. (6) and after applying square from both sides we have

$$V_{n+1}^2 = V_n^2 + 4V_n\epsilon_2\tilde{\omega}\sin(\tilde{\omega}\tilde{\Phi}) + 4\tilde{\omega}^2\epsilon_2^2\sin^2(\tilde{\omega}\tilde{\Phi}) - 4(V_n + 2\tilde{\omega})\sin(\tilde{\omega}\tilde{\Phi})\epsilon_1\sin(\phi_{n+1}) + 4\epsilon_1^2\sin^2(\phi_{n+1})$$

Concerning the above expression, let us consider an average in the interval $\phi \in [0, 2\pi]$ for all terms. So, the average is equal to zero for $\sin(\phi_{n+1})$ and $\sin(\tilde{\omega}\tilde{\Phi})$, and it is equal to 1/2 for the terms $\sin^2(\phi_{n+1})$ and $\sin^2(\tilde{\omega}\tilde{\Phi})$. Also, defining $\langle(\Delta V)^2\rangle = \overline{(V_{n+1})^2} - \overline{(V_n)^2}$, we finally end up with

$$\langle(\Delta V)^2\rangle = 2\tilde{\omega}^2\epsilon_2^2 + 2\epsilon_1^2 . \tag{8}$$

In our dynamical systems, the mapping is updated every time a collision with wall-1 occurs, which means that the smallest "time" interval that we have in our mapping dynamics, is the interval between collisions (n) and ($n+1$). So, considering the expression of $\langle(\Delta V)^2\rangle$ in the interval between collisions, that we may interpret as an infinitesimal interval for a derivative [12], one may set that

$$\frac{\overline{(V_{n+1})^2} - \overline{(V_n)^2}}{(n+1) - n} \approx \frac{\partial \overline{V^2}}{\partial n} . \tag{9}$$

Integrating both sides, we obtain

$$\int_{V_0}^{V_n} d\overline{V^2} = \int_0^n (2\tilde{\omega}^2\epsilon_2^2 + 2\epsilon_1^2)dn , \tag{10}$$

where one can end up with $\overline{(V_n)^2} = (V_0)^2 + (2\tilde{\omega}^2\epsilon_2^2 + 2\epsilon_1^2)n$.

For a better statistics, we set $V_{RMS} = \sqrt{\overline{V^2}}$. Then, an analytical expression for the velocity as a function of n is

$$V_{RMS} = \sqrt{(V_0)^2 + (2\tilde{\omega}^2\epsilon_2^2 + 2\epsilon_1^2)n}\,, \tag{11}$$

where V_0 is the initial velocity.

Of course this expression is not valid for any n, particularly the larger ones. Equation (11) is valid only for small n. Once the phase space is limited by invariant curves, an orbit in the low velocity regime cannot reach regions above the invariant curve for long time dynamics. If we literally take Eq. (11) as n is increased, V_{RMS} should also grow infinitely, and that is not what happens.

Now, let us move forward and discuss the numerical behavior for V_{RMS} and hence, compare the results with Eq. (11). We evaluated numerically the following expression

$$\overline{V^2} = \frac{1}{M}\sum_{i=1}^{M}\frac{1}{n}\sum_{j=1}^{n} {V_{i,j}}^2\,, \tag{12}$$

where M is the ensemble of initial conditions and n is the number of collisions. In a statistical point of view, we take the average of the velocity $V_{i,j}$ along the orbit running j and also along the ensemble of initial conditions running i. Initial conditions were always chosen in the chaotic sea with a low initial velocity $V_0 \approx \epsilon_{1,2}$ (always chosen by the smaller ϵ) and with the phase $\phi \in [0, 2\pi)$. This was made to guarantee a maximum diffusion for a chaotic particle.

Fig. 4 displays the behavior of some V_{RMS} curves as a function of n evaluated over an ensemble of 1000 initial conditions for different combinations of the control parameters ϵ_1, ϵ_2 and $\tilde{\omega}$. Each one of them was evolved up to 2×10^8 collisions. In Fig. 4(a,b) we have respectively $\tilde{\omega} = 1$ and $\tilde{\omega} = 10$ for six different combinations of ϵ_1 and ϵ_2.

For all curves displayed in Fig. 4 in the small n regime, the V_{RMS} curves start to grow, marked by a power law regime. Such growth is in agreement with the result obtained in Eq. (11), which shows that when n is small and considering a negligible initial velocity, i.e. $V_0 \cong 0$, all curves must diffuse with a $\sqrt{n}$. Hence, $V_{RMS} \propto n^{\beta}$, where $\beta \approx 1/2$. After the initial growth behavior, the V_{RMS} curves bend towards a crossover, characterized by n_x. Finally, for large enough n, all curves approach to a stationary state marked by a saturation plateau. Just for notice, the crossover n_x is obtained by the intersection of the steady state plateau with the growing power law curve, both marked by dashed lines in Figs. 4(a,b).

On the basis of the behavior shown in Figs. 4(a,b), where all curves of V_{RMS} present an initial power law growth for short times, passes through a crossover (n_x) and then bend towards a saturation plateau for really long times, we can suppose that the V_{RMS} curves behave as the following scaling hypothesis [54].

(i) For a small number of collisions, the behavior of V_{RMS} can be described by a power law of the type

$$V_{RMS} \propto n^{\beta}\,, \tag{13}$$

when we have $n \ll n_x$, where $\beta \approx 1/2$ is the growth exponent.

(ii) For a sufficient long n, the saturation plateau of V_{RMS} (we denote it as V_{sat}) is given by

$$V_{sat} \propto \epsilon_1^{\gamma_1}(\tilde{\omega}\epsilon_2)^{\gamma_2}\,, \tag{14}$$

for $n \gg n_x$, where both γ_1 and γ_2 are critical exponents.

(iii) Finally, the number of collisions that characterizes the changeover from growth to the saturation regime is given by

$$n_x \propto \epsilon_1^{z_1}(\tilde{\omega}\epsilon_2)^{z_2}\,, \tag{15}$$

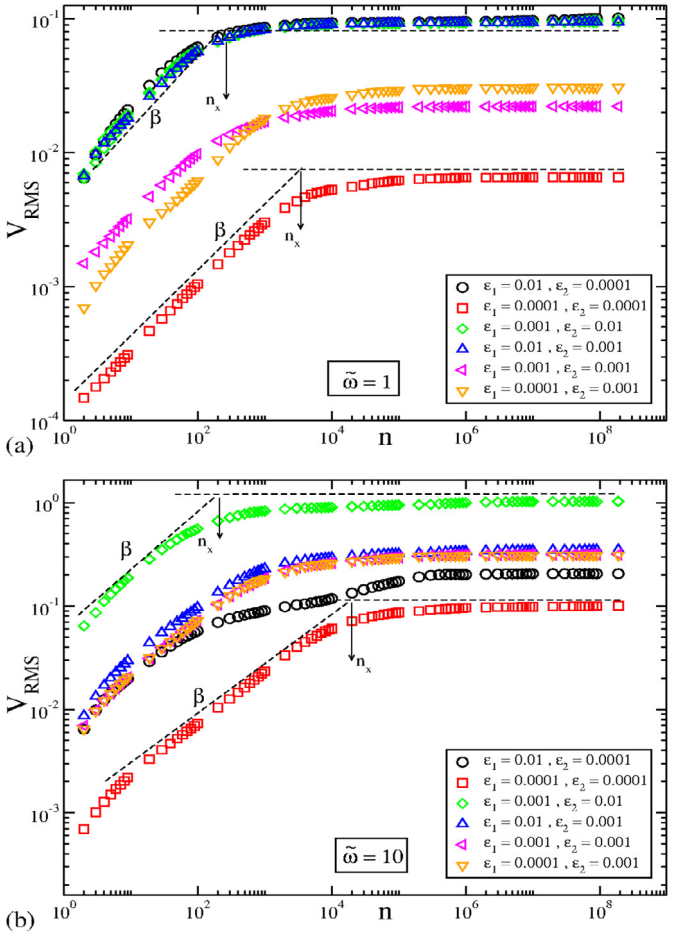

Fig. 4. Dynamical evolution of the V_{RMS} curves for different combinations of ϵ_1 and ϵ_2. In (a) we have $\tilde{\omega} = 1$ and in (b) $\tilde{\omega} = 10$. One can see that basically all curves follow the same behavior. An initial power law growth according to n^{β}, with $\beta \cong 0.5$, followed by a crossover n_x, where the curves then bend towards a steady state plateau for long times.

where n_x is the crossover collision, and z_1 and z_2 are called dynamical exponents.

One can notice that in the scaling arguments *(ii)* and *(iii)* the parameters ϵ_2 and $\tilde{\omega}$ appear together. They were proposed in this manner because of the mapping in Eq. (6), where both parameters always appear together in both mapping equations.

To obtain the critical exponents γ_1 and γ_2, we must evolve simulations concerning Eq. (12) for a very long time evolution. Thus, using extrapolation we can obtain the values of V_{sat} as functions of ϵ_1 and ϵ_2. Figs. 5(a,c) display the behavior of the value of V_{sat} in two different ways. First, in Fig. 5(a) we kept ϵ_2 constant as $\epsilon_2 = 0.0001$ and $\tilde{\omega} = 1$, and ranged ϵ_1, obtaining then $\gamma_1 = 0.502(5)$. Then, in Fig. 5(c), ϵ_2 was varied and we kept constant $\epsilon_1 = 0.001$ and $\tilde{\omega} = 10$ and we found that $\gamma_2 = 0.48(1)$. For both analysis in Figs. 5(a,c), we obtained that the exponents γ_1 and γ_2 have basically the same value $\cong 1/2$.

The exponents z_1 and z_2 shown in Fig. 5(b,d) were obtained by crossing the values obtained for the saturation and the initial growth regime as shown in Fig. 4. Again, in Fig. 5(b) ϵ_2 and $\tilde{\omega}$ were kept constant as $\epsilon_2 = 0.0001$ and $\tilde{\omega} = 1$ and we ranged ϵ_1, hence finding $z_1 = -0.97(1) \approx -1$. Finally, in Fig. 5(d), we ranged ϵ_2 and kept constant $\epsilon_1 = 0.001$ and $\tilde{\omega} = 10$ and thus obtained $z_2 = -1.07(1) \approx -1$. Also, the exponents z_1 and z_2 did not suffer any influence in the ranging of $\tilde{\omega}$.

It is worth emphasizing that the values of the exponents γ_1, γ_2, z_1 and z_2, are in remarkable agreement with the critical exponents

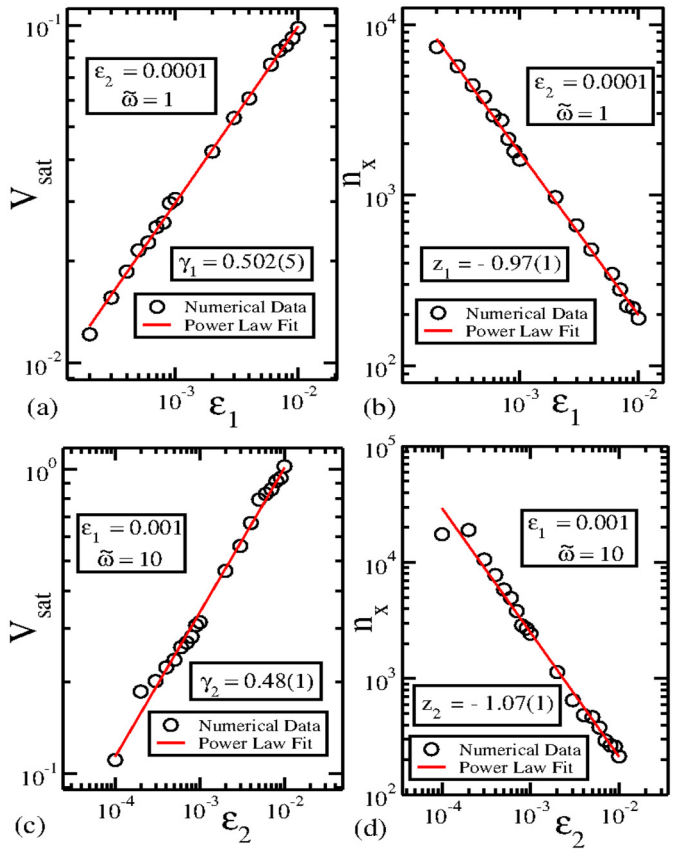

Fig. 5. In (a) plot of V_{sat} *vs* ϵ_1, for $\epsilon_2 = 0.0001$ and $\tilde{\omega} = 1$, resulting in $\gamma_1 = 0.502(5)$. In (b) plot of n_x *vs* ϵ_1, also for $\epsilon_2 = 0.0001$ and $\tilde{\omega} = 1$, yielding $z_1 = -0.97(1)$. In (c) plot of V_{sat} *vs* ϵ_2, for $\epsilon_1 = 0.001$ and $\tilde{\omega} = 10$, resulting in $\gamma_2 = 0.48(1)$. Finally in (d), plot of n_x *vs* ϵ_2, also for $\epsilon_1 = 0.001$ and $\tilde{\omega} = 10$, yielding $z_2 = -1.07(1)$.

obtained by the regular FUM (with one vibrating wall only) [52]. Such agreement gives validity and robustness to our numerical results and scaling arguments.

Now, in order to give robustness to our scaling hypothesis, let us describe the behavior of the V_{RMS} curves via a homogeneous generalized function [51,54] of the type

$$V(n, \epsilon_1, \tilde{\omega}\epsilon_2) = lV(l^a n, l^b \epsilon_1, l^c \tilde{\omega}\epsilon_2) , \tag{16}$$

where l is the scaling factor, and a, b and c are scaling exponents. Assuming that $l^a \tilde{\omega} n$ is constant, we have

$$l = n^{-1/a} . \tag{17}$$

Replacing Eq. (17) in (16), we have $V(n, \epsilon_1, \tilde{\omega}\epsilon_2) = n^{-1/a} V_1(1, l^{-b/a}\epsilon_1, l^{-c/a}\tilde{\omega}\epsilon_2)$, where V_1 is assumed to be constant for $n << n_x$. Hence, comparing with Eq. (13), we may find

$$\beta = -\frac{1}{a} . \tag{18}$$

Since $\beta \approx 1/2$, we obtain that $a \cong -2$.

Choosing now $l^b \epsilon_1$ constant, one may find

$$l = \epsilon_1^{-1/b} . \tag{19}$$

Substituting Eq. (19) in (16) we have $V(n, \epsilon_1, \tilde{\omega}\epsilon_2) = \epsilon_1^{-1/b} V_2(l^{-a/b} n, 1, l^{-c/b}\tilde{\omega}\epsilon_2)$, where V_2 is supposed to be constant for $n >> n_x$. Comparing with scaling hypothesis *(ii)* given in Eq. (14), we obtain

$$\gamma_1 = -\frac{1}{b} . \tag{20}$$

Following the same line, let us set now $l^c \tilde{\omega}\epsilon_2$ constant. So, we may obtain

$$l = (\tilde{\omega}\epsilon_2)^{-1/c} . \tag{21}$$

Replacing Eq. (21) in (16), one may find $V(n, \epsilon_1, \tilde{\omega}\epsilon_2) = (\tilde{\omega}\epsilon_2)^{-1/c} V_3(l^{-a/c} n, l^{-b/c}\epsilon_1, 1)$, where V_3 is also assumed to be constant for $n >> n_x$. Hence, one may compare the last expression with scaling hypothesis *(ii)* given in Eq. (14) and find

$$\gamma_2 = -\frac{1}{c} . \tag{22}$$

From the numerical values of γ_1 and γ_2 from Fig. 5, we may obtain that $b \cong -2$ and also $c \cong -2$.

Considering the analysis at the crossover, one can compare Eqs. (17) and (19) and obtain

$$n = \epsilon_1^{-a/b} . \tag{23}$$

Also, a comparison between Eqs. (17) and (21) gives us

$$n = (\tilde{\omega}\epsilon_2)^{-a/c} . \tag{24}$$

Comparing both above expressions with the scaling hypothesis *(iii)* given in Eq. (15), we find

$$-\frac{a}{b} = -\frac{a}{c} = z_1 = z_2 \cong -1 . \tag{25}$$

To check whether these initial suppositions are correct, let us now obtain a universal plot of different V_{RMS} curves. The behavior of V_{RMS} as a function of the number of collisions n for different values of the control parameters $\tilde{\omega}$, ϵ_1 and ϵ_2 is shown in Fig. 6(a). One can see that, after rescaling the coordinate axis according to the critical exponents obtained, all curves generate a single and universal plot, as shows Fig. 6(b). Such an universal plot, thus confirms the validity of the scaling hypothesis and gives robustness to the scaling invariance of the dynamics with respect to the control parameters.

3.2. Diffusion

When we consider transport properties and diffusion for chaotic dynamics [5,6], we can obtain the following expression

$$\langle [r(n) - r(0)]^2 \rangle = \int r(n)^2 \rho(\vec{r}, n) d\vec{r} = 2Dn , \tag{26}$$

where r is a generic action variable of the system dynamics, D is the diffusion coefficient, n is the iteration number and $\rho(\vec{r}, n)$ is the probability distribution of the system.

In the case of our two vibrating walls impact system, the generic action variable is now setup as the velocity of the particle. We can use the expression given by Eq. (26), together with the previously result obtained in Eq. (8), which is $\langle (\Delta V)^2 \rangle = 2\tilde{\omega}^2\epsilon_2^2 + 2\epsilon_1^2$. This procedure is made in order to obtain a numerical approximation for the diffusion coefficient. Thus, at each collision, we calculate the value of the root mean square velocity, as

$$\langle \Delta V^2 \rangle = \lim_{NP\to\infty} \frac{1}{NP} \sum_{i=1}^{NP} (V_n{}^i - V_0{}^i)^2 , \tag{27}$$

where NP is the number of particles (initial conditions), the index i denotes the NP particles and V_n is the velocity after n iteration of the ith particle. So, the diffusion coefficient [12], can be given as

$$D = \lim_{n\to\infty} \frac{1}{2n} \langle \Delta V^2 \rangle . \tag{28}$$

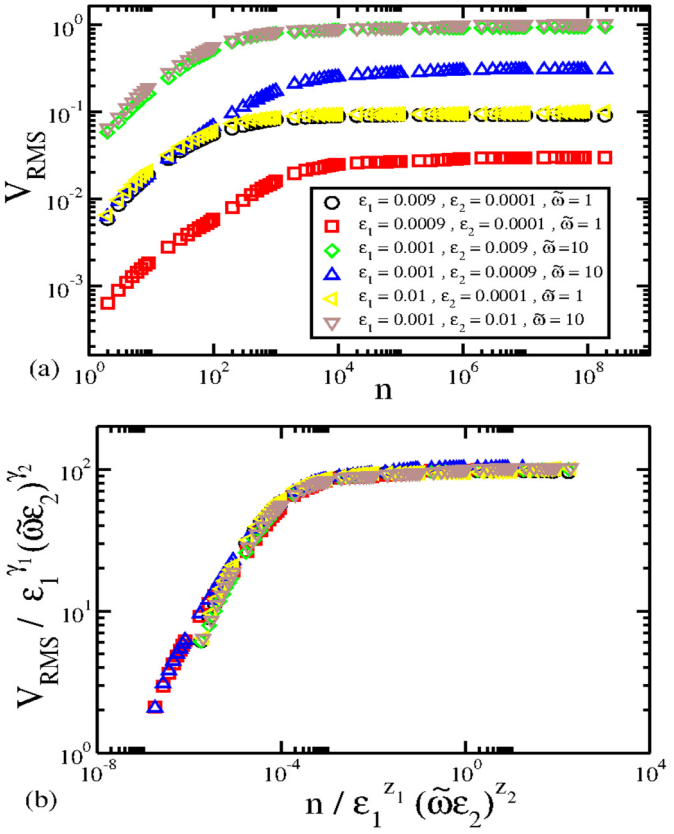

Fig. 6. In (a) plot of V_{RMS} curves for different combinations of $\tilde{\omega}$, ϵ_1 and ϵ_2. In (b) we have an universal overlap of all curves of (a) regarding the scaling arguments, confirming thus the scaling invariance with respect to the control parameters.

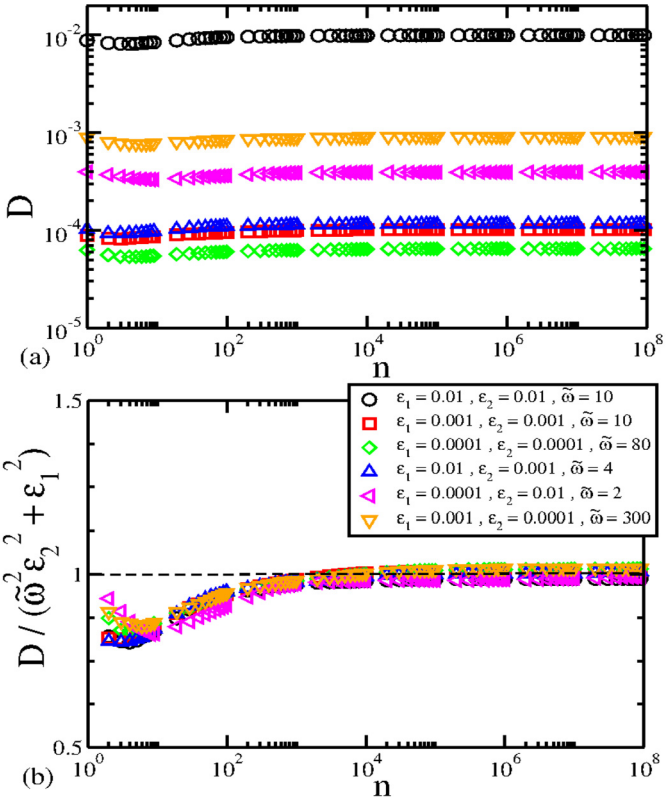

Fig. 7. In (a) we have the behavior of the diffusion coefficient D as function of n for different combinations of the control parameters. In (b), we have the collapse of all curves of (a) near the unity (dashed line), according Eqs. (8) and (27), which corroborates the robustness of our results.

Fig. 7(a) shows a plot of the diffusion coefficient obtained from Eq. (28) as function of n for $NP = 10^4$ for different combinations of the control parameters $\tilde{\omega}$, ϵ_1 and ϵ_2. The initial conditions were set uniformly distributed along the phase $\phi \in [0, 2\pi)$, and the initial velocity was set always regarding the lower value of ϵ_1 or ϵ_2. One can see that basically the diffusion sustains itself in a constant plateau as the number of collision evolves.

In Fig. 7(b), when we compare the relation between the diffusion coefficient and $\langle(\Delta V)^2\rangle$, we can see that all diffusion curves collapse themselves near the unity line (dashed line), after a rescaling in the vertical axis according $\tilde{\omega}^2\epsilon_2^2 + \epsilon_1^2$, thus confirming what was foreseen by the analytical analysis of the root mean square velocity. This result remarkably corroborates the linear dependence between D and $\tilde{\omega}^2\epsilon_2^2 + \epsilon_1^2$, as predicted by Eq. (8) and gives robustness to our numerical results.

4. Final remarks and conclusions

To summarize, we introduced the study of the dynamics of a particle confined between two heavy walls, where both are periodically perturbed. The dynamics was described by an original, two-dimensional, nonlinear and area preserving mapping, which has three control parameters and four nonlinear terms. The phase space is composed by chaotic seas, KAM islands and invariant tori, which separate different regions in the phase space. The major chaotic sea portion regards the value of the bigger perturbation parameter. The amount of KAM islands in the phase space is proportional to the value of the ratio between the frequencies of oscillation of the two vibrating walls ($\tilde{\omega}$), i.e., for a certain region of the phase space, for $\tilde{\omega} = 2$ we have a chain of two islands and for $\tilde{\omega} = 10$, one may find a chain of ten KAM islands. Also, their cantori and satellite islands also obeys $\tilde{\omega}$ in a linear way (as shown in Fig. 3).

Analyzing the expression for the root mean square velocity, we estimated analytically the behavior of V_{RMS}. For short times, the curves grow according $\sqrt{n}$, and then after a crossover, they bend towards a steady state plateau for long times. Scaling hypothesis were proposed to describe the behavior of the V_{RMS} curves as function of the control parameters. We were able to obtain an universal collapse regarding these scaling hypothesis, thus confirming their validity. Also, concerning the diffusion coefficient, numerical simulations were made and show a remarkable agreement with the analytical expression for $\langle(\Delta V)^2\rangle$, confirming the relation between the diffusion coefficient and $\tilde{\omega}^2\epsilon_2^2 + \epsilon_1^2$ as predicted by Eq. (8).

In the near close future, we would like to investigate the role of the $\tilde{\omega}$ parameter as a irrational number, the introduction of uncorrelated phases between the vibrating walls, as well as investigation of anomalous transport and stickiness influence. Also, the introduction of dissipation in the dynamics via restitution coefficients in both walls, seems to be promising in order to observe chaotic attractors, crises between manifolds and self similarity structures in the parameter space.

Acknowledgements

ALPL acknowledges FAPESP (2014/25316-3), FAPESP (2015/26699-6) and CAPES for financial support. The author also thanks Edson D. Leonel, Iberê L. Caldas, Carl P. Dettmann for fruitful discussions, and acknowledges the University of Bristol for the kindly hospitality during his stay in UK. This research was supported by resources supplied by the Center for Scientific Computing (NCC/GridUNESP) of the São Paulo State University (UNESP).

The author also thanks Mirian Castejon Molina for the production of Fig. 1.

References

[1] R.C. Hilborn, Chaos and Nonlinear Dynamics: An Introduction for Scientists and Engineers, Oxford University Press, New York, 1994.
[2] A.J. Lichtenberg, M.A. Lieberman, Regular and Chaotic Dynamics, Appl. Math. Sci., vol. 38, Springer Verlag, New York, 1992.
[3] G.M. Zaslasvsky, Physics of Chaos in Hamiltonian Systems, Imperial College Press, New York, 2007.
[4] G.M. Zaslasvsky, Hamiltonian Chaos and Fractional Dynamics, Oxford University Press, New York, 2008.
[5] P. Gaspard, Chaos, Scattering and Statistical Mechanics, Cambridge University Press, Cambridge, 1998.
[6] R.K. Pathria, Statistical Mechanics, Elsevier, Burlington, 2008.
[7] A.L.P. Livorati, T. Kroetz, C.P. Dettmann, I.L. Caldas, E.D. Leonel, Phys. Rev. E 86 (2012) 036203.
[8] T. Kroetz, A.L.P. Livorati, E.D. Leonel, I.L. Caldas, Phys. Rev. E 92 (2015) 012905.
[9] A.L.P. Livorati, I.L. Caldas, C.P. Dettmann, E.D. Leonel, Phys. Lett. A 379 (2015) 2830.
[10] G. Diaz-I, A.L.P. Livorati, E.D. Leonel, Phys. Lett. A 380 (2016) 1830.
[11] A.L.P. Livorati, M.S. Palmero, C.P. Dettmann, I.L. Caldas, E.D. Leonel, J. Phys. A 47 (2014) 365101.
[12] A.L.P. Livorati, C.P. Dettmann, I.L. Caldas, E.D. Leonel, Chaos 25 (2015) 103107.
[13] J.A. Méndez-Bermúdez, A.J. Martínez-Mendoza, A.L.P. Livorati, E.D. Leonel, J. Phys. A 48 (2015) 405101.
[14] S.M. Ulam, A Collection of Mathematical Problems, Interscience Tracts in Pure and Applied Mathematics, vol. 8, Interscience Publishers, New York–London, 1960.
[15] E. Fermi, Phys. Rev. 75 (1949) 1169.
[16] N. Chernov, R. Markarian, Chaotic Billiards, American Mathematical Society, vol. 127, 2006.
[17] A. Loskutov, A.B. Ryabov, L.G. Akinshin, J. Phys. A 33 (2000) 7973.
[18] P. Dainese, P.St.J. Russell, N. Joly, J.C. Knight, G.S. Wiederhecker, H.L. Fragnito, V. Laude, A. Khelif, Nat. Phys. 2 (2006) 388.
[19] M. Scheel, R. Seemann, M. Brinkmann, M. Di Michiel, A. Sheppard, B. Breidenbach, S. Herminghaus, Nat. Mater. 7 (2008) 189.
[20] L. Sirko, P.M. Koch, R. Blümel, Phys. Rev. Lett. 78 (1997) 2940.
[21] F. Haake, Quantum Signatures of Chaos, Springer, Berlin, 2001.
[22] L.A. Ponomarenko, F. Schedin, M.I. Katsnelson, R. Yang, E.W. Hill, K.S. Novoselov, A.K. Geim, Science 320 (2008) 356.
[23] L. Meza-Montes, S.E. Ulloa, Phys. Rev. E 55 (1997) R6319.
[24] A.C.J. Luo, R.P.S. Han, Nonlinear Dyn. 10 (1996) 1.
[25] J.J. Barroso, M.V. Carneiro, E.E.N. Macau, Phys. Rev. E 79 (2009) 026206.
[26] A.D. Stone, Nature 465 (2010) 696.
[27] T.L. Vincent, A.I. Mees, Int. J. Bifurc. Chaos 10 (2000) 579.
[28] T.L. Vincent, Nonlinear Dyn. Syst. Theory 1 (205) (2001).
[29] A. Veltri, V. Carbone, Phys. Rev. Lett. 92 (2004) 143901.
[30] F. Saif, I. Bialynicki-Birula, M. Fortunato, W.P. Schleich, Phys. Rev. A 58 (1998) 4779.
[31] A. Steane, P. Szriftgiser, P. Desbiolles, J. Dalibard, Phys. Rev. Lett. 74 (1995) 4972.
[32] S.T. Dembinski, A.J. Makowski, P. Peplowski, Phys. Rev. Lett. 70 (1993) 1093.
[33] J.V. José, R. Cordery, Phys. Rev. Lett. 56 (1986) 290.
[34] Z.J. Kowalik, M. Franaszek, P. Pieranski, Phys. Rev. A 37 (1988) 4016.
[35] S. Warr, W. Cooke, R.C. Ball, J.M. Huntley, Physica A 231 (1996) 551.
[36] A.K. Karlis, P.K. Papachristou, F.K. Diakonos, V. Constantoudis, P. Schmelcher, Phys. Rev. Lett. 97 (2006) 194102.
[37] A.K. Karlis, P.K. Papachristou, F.K. Diakonos, V. Constantoudis, P. Schmelcher, Phys. Rev. E 76 (2007) 016214.
[38] A.K. Karlis, F.K. Diakonos, V. Constantoudis, P. Schmelcher, Phys. Rev. E 78 (2008) 046213.
[39] O.F. De Alcantara Bonfim, Int. J. Bifurc. Chaos 22 (2012) 1250140.
[40] S. Denisov, S. Flachc, Peter Hänggi, Phys. Rep. 538 (2014) 77.
[41] N.A.C. Hutchings, M.R. Isherwood, T. Jonckheere, T.S. Monteiro, Phys. Rev. E 70 (2004) 036205.
[42] J. Rosa, M.W. Beims, Phys. Rev. E 78 (2008) 031126.
[43] Y.K. Bae, AIAA SPACE Conf. and Expo. (2007) 6156.
[44] Y.K. Bae, AIP Conf. Proc. 813 (2006) 1213.
[45] Y.K. Bae, Phys. Proc. 38 (2012) 253.
[46] S. Fishman, D.R. Grempel, R.E. Prange, Phys. Rev. Lett. 49 (1982) 509.
[47] B.G. Klappauf, W.H. Oskay, D.A. Steck, M.G. Raizen, Phys. Rev. Lett. 81 (1998) 4044.
[48] P.H. Jones, M.M. Stocklin, G. Hur, T.S. Monteiro, Phys. Rev. Lett. 93 (2004) 223002.
[49] M.M.A. Stocklin, T.S. Monteiro, Phys. Rev. E 74 (2006) 026210.
[50] T.S. Monteiro, A. Rançon, J. Ruostekoski, Phys. Rev. Lett. 102 (2009) 014102.
[51] A.L.P. Livorati, D.G. Ladeira, E.D. Leonel, Phys. Rev. E 78 (2008) 056205.
[52] E.D. Leonel, P.V.E. McClintock, J.K.L. da Silva, Phys. Rev. Lett. 93 (2004) 014101.
[53] D.F. Tavares, E.D. Leonel, R.N. Costa Filho, Physica A 391 (2012) 5366.
[54] A-L. Barabasi, H.E. Stanley, Fractal Concepts in Surface Growth, Cambridge University Press, New York, 1995.